Fractal Characteristics of Pore Structure of Gas Shale: A Case Study of Lower Silurian Longmaxi Formation

Yiqiang Pan

Department of Engineering Technology Management, International College, Krirk University, Bangkok 10220, Thailand, 2010902@cqust.edu.cn

Knowing pore structure is crucial to estimate the properties of gas shale. To characterize the pore structure and fractal feature of the Lower Silurian Longmaxi Formation in the northeast of Chongqing Municipality, China, three methods, including low pressure nitrogen adsorption (LPNA) and mercury intrusion porosimetry (MIP) as well low-field nuclear magnetic resonance (NMR), were conducted to research the fractal characteristics of pore structure. We analyzed and discussed the test results, pore size distribution and fractal dimensions based on different experimental methods. These results demonstrate that the sample in this work is composed of plate-like particles, and there exists an abundance of mesopores. The LPNA method is suitable for testing the diameter characteristics of micropores and mesopores, the MIP means is appropriate for characterizing the pore diameter of macropores, and the NMR method is better at identifying the nuclear magnetic signals of hydrogen atoms present in micropores, mesoporous and macropores. The fractal dimension increase with pore diameter increasing, revealing the heterogeneity of pores from small to big is in this order: micropores, mesopores and macropores. This study investigates the fractal characteristics of the pore structure of gas shale from lower Silurian Longmaxi formation and offers a potential path for accurately characterizing the full-scale characteristics of gas shale pore structure to make full use of the advantages of LPNA, MIP and NMR.

Keywords: Fractal characteristics, Pore structure, Longmaxi gas shale, LPNA, MIP, NMR.

1. INTRODUCTION

Since the US shale gas revolution, shale gas has been one of the hot research topics for many

scholars all over the world [1-4]. Especially, the pore structure of gas shale becomes an important area for illustrating the particularity of shale gas adsorption/ desorption [5], transport [6] and diffusion [7]. Therefore, many publications have been pressed to characterize the pore structure of gas shale. Nowadays, the fractal theory become a means of great significance to reveal the characteristics of pore structure of gas shale, which is much more complicated than conventional oil or gas reservoirs.

Many works have been done for investigating the role of pore structure during the processes of shale gas exploration and development. Yuan et al. [8] quantified the impact of clay and total organic carbon (TOC) contents on micro-/mesopore volume, surface area, and pore size distribution (PSD) using three shale formations with large compositional variations. Shi et al. [9] studied the intrinsic relationship between organic matter graphitization degree, organic matter, pore structure parameters, and shale porosity. Zhao et al. [10] studied the reliability of NMR-based porosity, and gave some offers on how to increase the reliability of NMR-based porosity of shale sample. Hou et al. [11] experimentally study on the spontaneous imbibition mechanism with ultra-low IFT in oil-wet shale oil reservoirs by NMR.

Furthermore, some different methods have been conducted to characterize the pore structure of gas shale. Sun et al. [12] studied the pore structure of gas shale outcrops from the Lower Silurian Longmaxi Formation by using field emission scanning electron microscope (FE-SEM). Li et al. [13] researched the fractal characteristics and pore structure of Lower Cambrian Qiongzhusi formation in eastern Yunnan Province, South China by using the fractal Frenkele-Halseye-Hill (FHH) method based on the nitrogen adsorption experiment data. Li et al. [14] characterized the fractal feature and pore structure of continental and marine shale based on N_2 adsorption, mercury porosimetry and NMR methods. Cao et al. [15] characterized the fractal feature and pore structure of Paleozoic shales from the northeast of Sichuan Basin, China.

In this work, three experimental methods, including Low pressure N_2 adsorption, mercury intrusion porosimetry and nuclear magnetic resonance, were conducted to illustrate the fractal characteristics and pore structure of lower Silurian Longmaxi gas shale, which has the maximum gas production capacity in China. These results would be very meaningful for understanding the applicability of different experimental methods, and meaningful for characterizing the fractal pore structure of gas shale.

2. Material and Research Method

2.1 Sample preparation

The Sichuan Basin is tectonically located in the northwest of the Yangtze metaplatform and surrounded by the Yunnan–Guizhou–Sichuan–Hubei platform fold zone [16]. The lithology of Longmaxi member is siliceous shale and mudstone with high organic matter content, which is the main shale gas producing section [17]. The rock samples used in this study were selected from an exploratory well in the northeast of Chongqing City, China, at a depth of about 1072 m. 60 - 120 mesh shale powders were selected and dried in an oven at 60 ° C till powder weight is stable. After drilled and dried, the cylindrical core was tested for porosity and permeability, followed by mercury injection test. Meanwhile, the massive rock sample

was selected, dried and then used for low-field nuclear magnetic resonance experiment.

2.2 Methods

2.2.1 Low pressure N_2 adsorption method

Low pressure N_2 adsorption (LPNA) can be applied to evaluate the pore structure of gas shale at the condition of -196 ℃ and 127 kPa. The powered samples were dried in an oven to remove moisture. Then 4 g of the samples were selected and uploaded in the apparatus for analysis. The pore size distribution was tested by ASIQM00002000-7. The curves of isothermal adsorption and desorption were obtained through measurement.

In recent years, several methods, including fractal BET model [18], fractal FHH model [19] and the thermodynamic model [20], have been deduced to recognize the fractal characteristics of oil or gas shale by using the data from the Low Pressure N_2 Adsorption test. The FHH model based on LPNA data [21-22] is as follows [23]:

$$\ln(V) = C + (D-3)\ln\left(\ln\left(\frac{P_0}{P}\right)\right) \quad (1)$$

where V is the volume of nitrogen adsorbed at each equilibrium pressure in cm^3/g; p is the equilibrium pressure in MPa; p_0 is the saturation pressure in MPa; C is a constant; and D is the fractal dimension. Thus, according to Eq.(1), ln(V) should be linearly positively correlated with $\ln(\ln(p_0/p))$, and then parameter D can be deduced by the slope.

2.2.2 Mercury intrusion porosimetry

Mercury intrusion porosimetry (MIP) is a classic method to study the pore size distribution and structure [24]. The fractal dimension of MIP results is discussed by Li et al. [14], and its equation can be shown as follows [14]:

$$\lg(S) = (D-3)\lg(P) + (D-3)\lg(P_{min}) \quad (2)$$

where S is the cumulative porosity fraction of pores with less pore radius r, P is the capillary pressure in MPa, P_{min} is the minimum of capillary pressure in MPa. lg(S) should be positively linearly correlated with lg(P), and then parameter D can be obtained by the slope.

2.2.3 Low-field nuclear magnetic resonance

Low-field nuclear magnetic resonance (NMR) is a non-destructive method, and has been widely used in the exploration and development of oil or gas fields [25]. The NMR experiments were conducted by using a MacroMR12-150H-1 analyzer manufactured by Shanghai Niumai Corporation to read and save the T_2 spectrum of the water in the shale cores. The specific device parameters are shown as follows [26]: The magnetic field strength was 0.3±0.05 t. The pulse frequency ranges from 2 MHZ to 30mhz. The shortest echo time is less than 60 μs. The fractal dimension of pore structure from NMR was discussed with the reference to Shao et al. [27], and the cumulative volume fraction with transverse relaxation times less than T2 is calculated as follows [15]:

$$\lg(V) = (3-D)\lg(T_2) + (D-3)\lg(T_{2\,max}) \quad (3)$$

where V is the cumulative volume fraction with transverse relaxation times less than T_2 in μm^3, T_2 is the transvers relaxation time, and T_{2max} is the biggest value of transvers relaxation time. Thus, according to Eq.(3), the relationship between lg(V) and lg(T_2) should be positively linear, and then parameter D can be determined by the slope.

To characterize the pore structure of gas shale samples from the Lower Silurian Longmaxi Formation, the workflow was described as the following: (1) The massive shale samples were vacuumed down to 10^{-5} Pa by a vacuum pump, and saturated 2% KCL solution for 24 hours. (2) The T_2 spectra of sample was tested. (3) Analyze the shale pore size distribution based on the data of T_2.

3. Results and Analysis

3.1 Experimental results

3.1.1 The results of LPNA [28]

The relationships between nitrogen adsorption or nitrogen desorption and relative pressure are shown in Fig. 1. Clearly seen that there is an obvious hysteresis phenomenon between desorption and adsorption isotherms same as previous publications [29-30]. According to the types of physical adsorption isotherms and hysteresis loops classified by Sing, the LPNA curve of the shale sample belongs to type II isotherms, reflecting that the middle of the near-linear isotherm begins with the completion of single-layer coverage and multi-layer adsorption begins. The hysteresis loops are identified as type H3, indicating that the sample is composed of plate-like particles and forms cracks.

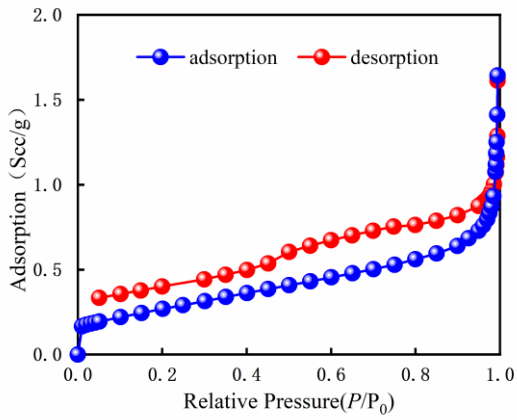

Fig. 1. The isothermal adsorption and desorption curves

3.1.2 The results of MIP

The result of MIP is shown as in Fig. 2, and the relationship between capillary pressure and saturation of mercury is depicted. It can be seen that there are two curve branches: intrusion branch and extrusion branch, and there exists an obvious entrapment between the two branches, reflecting that much mercury is trapped in the shale sample after experiment test.

The capillary pressure reaches to the value of 411.59 MPa while the maximum mercury saturation is 39.87% which is much lower than 100% because the limit of the maximum pressure of mercury injection, and some smaller pores can not be entered [31]. The specific surface area is 722.73 cm^3/g.

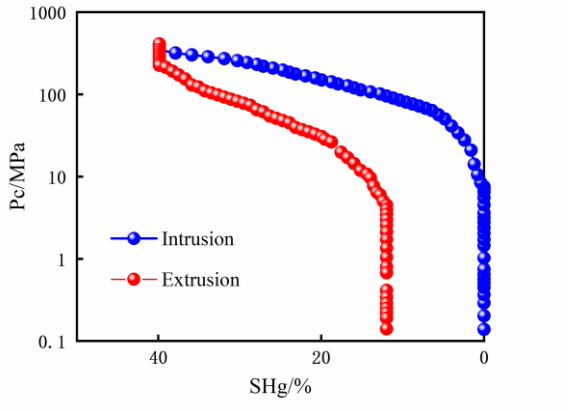

Fig. 2. The mercury intrusion porosimetry curves

3.1.3 The results of NMR

The curve of amplitude versus T_2 is plotted in Fig. 3. Obviously shown is that there exist three peaks in the nuclear magnetic curve, and from the left to the right, the first peak is the highest, the second one is in the middle, and the third one is the lowest. This phenomenon can be observed in other publications [32-33]. Furthermore, the three peaks from left to right can be respectively seen as the small pores, big pores and microfractures. The amplitude of small pores mainly distributes from 0 to 338.27, big pores range chiefly is between 0 and 64.65, and the microfractures range primarily is between 0 and 21.98.

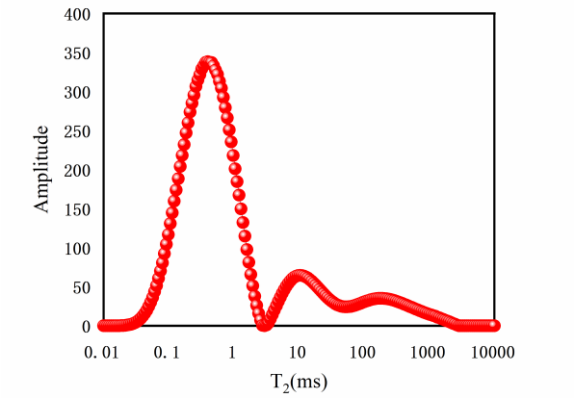

Fig. 3. The nuclear magnetic resonance curve

3.2 Pore size distribution of different experiments

3.2.1 Pore size distribution of LPNA

The ratio of pore volumes with different diameters to total pore volume is served as the frequency in this section, and the curve of the frequency and pore diameter is depicted as Fig. 4 (a). Clearly seen is that the frequency first increases, then decreases, and gradually becomes stable although there are small fluctuations. Furthermore, pore diameter distributes from 1.56 to 77.70 nm, and the peak of frequency lies in pore diameter of 4.25 nm. The pore volume of micropore ($d \leq 2$ nm), mesopore ($2 < d \leq 50$ nm) and macropore ($d > 50$ nm) accounted for 1.7%, 86.76% and 11.54% of the total pore volume, respectively, indicating that there exists a lot of mesopores for this gas shale sample from lower Silurian Longmaxi formation.

3.2.2 Pore size distribution of MIP

The ratio of the different volume of mercury injected in pore volume with different diameters to total volume of mercury injected is defined as the frequency in this section, and the relationship between the diameter and its frequency are plotted as Fig. 4 (b). The frequency increases and then decreases with diameter increasing, and the maximum frequency is 3.0 as the diameter rises to 74.40 nm. Furthermore, pores smaller than 2nm in diameter could not be detected, and the diameter distributes from 6.53 to 421.61 nm. The pore volume of mesopores ($2 < d \leq 50$ nm) and macropores ($d > 50$ nm) accounted for 71.43% and 28.57% of the total pore volume, respectively, indicating that the mesopores takes up the majority for this gas shale sample from lower Silurian Longmaxi formation.

3.2.3 Pore size distribution of NMR

The value of amplitude of different T_2 divided by cumulative amplitude is used as the frequency to depict the pore size distribution of gas shale sample saturated with 2% KCL, and the relationship between the frequency and the diameter was plotted as Fig. 4 (c). Obviously seen is that three main pore types occupy the majority of pores according to the three peaks in the curve. Specifically, the frequency for highest peak is 2.4120% while the diameter arrives at 7.4048 nm, the second frequency is 0.4610% as the diameter is 33.6981 nm, and the frequency of lowest peak is 0.2507% when the diameter equals to 126.3827nm. Furthermore, the pore volume of micropore ($d \leq 2$ nm), mesopore ($2 < d \leq 50$ nm) and macropore ($d > 50$ nm) accounted for 0.02%, 88.40% and 11.58% of the total pore volume, respectively, indicating that there exists an abundance of mesopores lower Silurian Longmaxi formation in northeast of Chongqing Municipality, China.

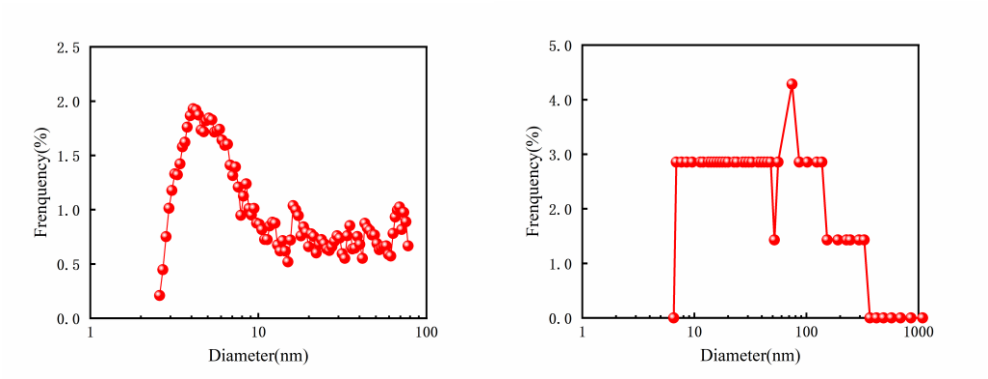

(a) LPNA (b) MIP

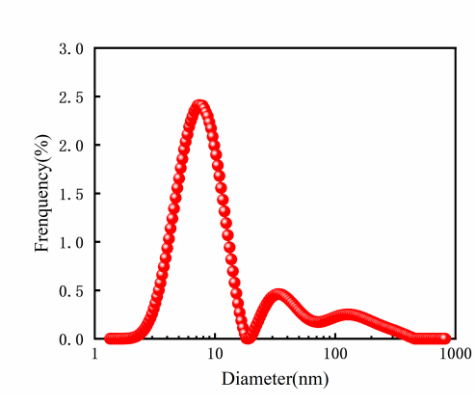

(c) NMR

Fig. 4. The relationship between frequency and pore diameter

3.3 Fractal dimensions obtained by different methods

3.3.1 Fractal dimensions obtained by LPNA

According to Eq.(1), the linear relationship between ln(V) and ln(ln(P_0/P)) was obtained by fitting experimental data with different pore diameter intervals, and the plot was shown as Fig. 5. It can be seen that ln(V) is linearly negatively related with ln(ln(P_0/P)) within different pore diameter intervals. Specifically, the fitting equation is shown as y=-0.4015x-1.1937 as the pore diameter is from 1.7266 to 1.9852 nm, and the correlation coefficient (R^2) is 0.9890. Then, the linear equation is as y=-0.2719x-1.0686 while the pore diameter distributes from 2.0745 to 40.4200 nm, and the correlation coefficient (R^2) is 0.9726. Furthermore, according to the slopes of fitting results and Eq.(1), the fractal dimensions of two linear phases can be calculated as 2.5985 and 2.7281, respectively. Namely, the fractal dimension of mesopores is greater than that of micropores, reflecting that the heterogeneity of mesopores is stronger than micropores for Longmaxi gas shale formation by using LPNA method.

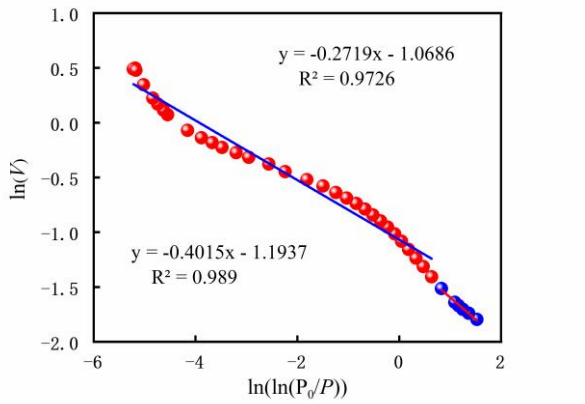

Fig. 5. The fracture curves of low pressure N_2 adsorption

3.3.2 Fractal dimensions obtained by MIP

According to Eq.(2), the fitting results between lg(S_{Hg}) and lg(P_c) is shown as Fig. 6 with different pore diameter intervals. Obviously seen that there are two linear phases, and there exists a good linear positive correlation between lg(S_{Hg}) and lg(P_c) in each phase. Specifically, as the pore diameter distributes from 9.4410 to 43.1877 nm, the linear fitting equation is as y=1.2886x-1.4856, and the correlation coefficient (R^2) is 0.9913. Meanwhile, the fitting result is as y=0.8762x-0.6196 when the pore diameter ranges from 51.0218 to 2949.3628 nm, and the correlation coefficient (R^2) is 0.9943. Furthermore, according to the slopes of fitting results and Eq.(2), the fractal dimensions of two linear phases can be calculated as 1.7114 and 2.1238, respectively. Namely, the fractal dimension of mesopores is smaller than that of macropores, meaning that the heterogeneity of macropores is much stronger than mesopores for Longmaxi gas shale formation by using MIP method.

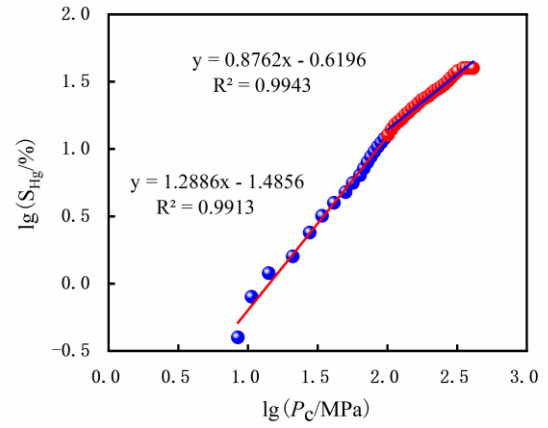

Fig. 6. The fracture curves of mercury intrusion porosimetry

3.3.3 Fractal dimensions obtained by NMR

By using Eq.(3) and NMR data, the relationship between lg(V) and lg(T_2) was fitted as shown in Fig. 7, and there are three linear phases in the curve of nuclear magnetic resonance according to the different pore types. Specifically, while the pore diameter ranges from 1.3409 to 1.9744 nm, the fitting equation is as y=9.9437x+14.744, and the correlation coefficient (R^2) equals to 0.9806. Then, the fitting result is shown as y=0.8533x+1.4124 when the pore diameter distributes from 2.0391 to 49.6169 nm, and the correlation coefficient (R^2) is 0.6890. Moreover, as the pore diameter is between 51.2426 and 444.3918 nm, the fitting equation is y=0.0281x+1.9112, and the correlation coefficient (R^2) is 0.9746. These results reflect that there exist good linear relationship between lg(V) and lg(T_2) with different pore diameter distribution intervals, and the correlation of micropores is the best and the correlation of mesopores is the least. Furthermore, based on the Eq.(3) and the fitting equations, the fractal dimensions are -6.9437, 2.1467 and 2.9719, reflecting that the heterogeneity of pores is in this order from big to small: macropores, mesopores and micropores by analyzing the NMR data.

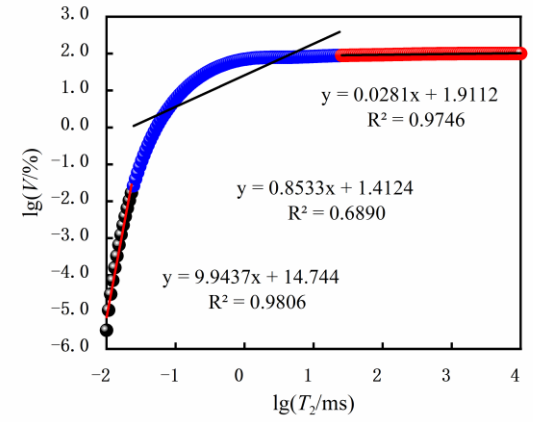

Fig. 7. The fracture curve of nuclear magnetic resonance

3.4 Discussion

3.4.1 Pore size distribution from different measurement methods

To better understand the pore size distribution of gas shale and the advantages or disadvantages of different measurement means, the pore size distribution from different measurement means are compared in Fig. 8. Clearly seen that the pore size distribution intervals measured by NMR is the widest, namely the diameter distribution intervals measured by both MIP and LPNA are all narrower than that measured by NMR. Specifically, when the pore diameter is within the macropore interval, there exists more consistent trends between MIP and NMR methods. Meanwhile, as the pore diameter is within the micropores and mesopores intervals, the curve tendencies of LPNA and NMR are more consistent. Therefore, the LPNA method is suited for testing the pore structure characteristics of micropores and mesopores, the MIP means is appropriate for characterizing the pore diameter of macropores, and the NMR method is better at identifying the nuclear magnetic

signals of hydrogen atoms present in micropores, mesoporous and macropores. Furthermore, it is a potential path for accurately characterizing the full-scale characteristics of gas shale pore structure to make full use of the advantages of LPNA, MIP and NMR.

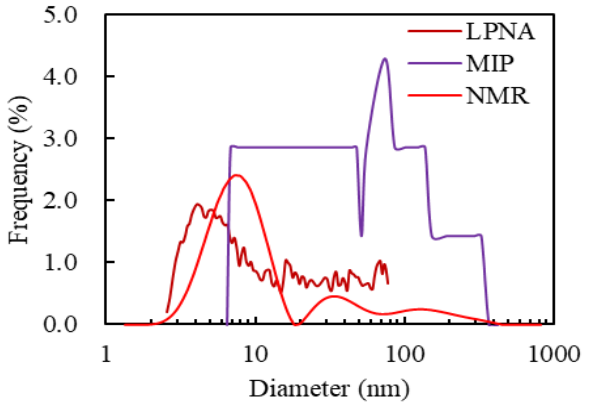

Fig. 8. The pore diameter frequency from different measurement methods

3.4.2 Fractal dimensions from different measurements methods

To understand the fractal characterize of gas shale pore structure, the fractal dimensions of different diameter range were depicted in Fig. 9. Clearly seen is that the fractal dimensions increase with the diameter increasing, which is same as the previous work [34]. Specifically, for LPNA method, the fractal dimension of mesopores is greater than micropores. Meanwhile, the fractal dimension of mesopores is smaller than macropores for MIP measurement. Finally, for NMR test, the fractal dimensions from small to big is in this order: micropore, mesopores and macropores. Furthermore, the fractal dimension of micropores obtained by NMR is different because the value is smaller than zero, which is different because it is designed to reveal the fractal dimensions of different pore types within the different pore diameter intervals, and some other scholars divided the pore into two types: adsorption pores and seepage pore and studied their fractal feature [14] [35]. Therefore, this navigate fractal dimension of micropores still needs further research for fractal theory in the field of studying the pore size distribution in porous media. These results reflect that heterogeneity of pores from small to big is in this order: micropores, mesopores and macropores, for Longmaxi gas shale in the northeast of Chongqing Municipality, China.

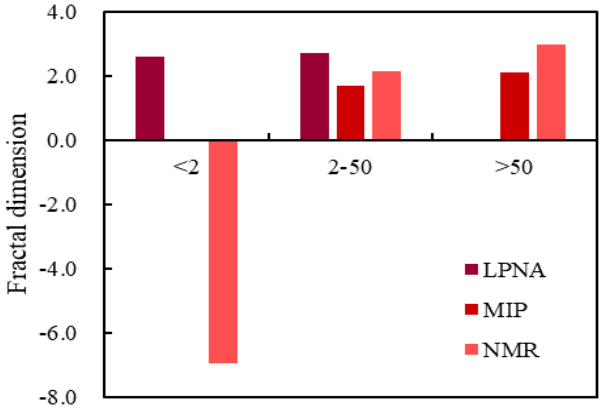

Fig. 9. Fractal dimension of different diameter range from different measurement methods

4. Conclusions

The gas shale from lower Silurian Longmaxi formation in this work is composed of plate-like particles which caused the slit-shaped pores, and there exists an abundance of mesopores.

Different methods have different application for studying the fractal characteristics of pore structure of gas shale. The LPNA method is suited for testing the pore size distribution of micropores and mesopores, the MIP means is appropriate for characterizing the pore size distribution of macropores, and the NMR method is better at identifying the nuclear magnetic signals of hydrogen atoms present in micropores, mesoporous and macropores.

The fractal dimensions increase with pore diameter increasing. For LPNA method, the fractal dimension of mesopores is greater than micropores. The fractal dimension of mesopores is smaller than macropores for MIP measurement. For NMR test, the fractal dimensions from small to big is in this order: micropore, mesopores and macropores. The heterogeneity of pores from small to big is in this order: micropores, mesopores and macropores for Longmaxi gas shale in the northeast of Chongqing Municipality, China.

Acknowledgement

This research did not receive any specific grant from funding agencies in the public, commercial, or not-for-profit sectors.

References

1. N. J. Kuang, J. P. Zhou, X. F. Xian, C. P. Zhang, K. Yang, Z. Q. Dong, “Geomechanical risk and mechanism analysis of CO2 sequestration in unconventional coal seams and shale gas reservoirs”, Rock Mechanics Bulletin, vol. 2, no. 4, pp. 100079, 2023. https://doi.org/10.1016/j.rockmb.2023.100079
2. H. Qu, S. Tang, Z. Liu, J. Mclennan, R. Wang, “Experimental investigation of proppant

particles transport in a tortuous fracture", Powder Technology, vol. 382, pp. 95-106, 2020. https://doi.org/10.1016/j.powtec.2020.12.060

3. S. Kim, T. W. Kim, Y. Hong, J. Kim, H. Jeong, "Enhancing pressure gradient prediction in multi-phase flow through diverse well geometries of North American shale gas fields using deep learning", Energy, vol. 290, pp. 130291, 2024. https://doi.org/10.1016/j.energy.2024.130291
4. N. D. Arenas Zapata, G. B. Savioli, J. E. Santos, P. M. Gauzellino, "Numerical simulation of fracking and gas production in shale gas reservoirs", Geophysical Prospecting, vol. 72, no. 3, pp. 1133-1145, 2024. https://doi.org/10.1111/1365-2478.13462
5. Y. Wang, Y.L. Zhang, T. Dong, K. Duan, J.H. Wen, H. Zhang, T. Xie, F. Luo, "Pore Structure and Fractal Characteristics of the Middle and Upper Permian Dalong and Gufeng Shale Reservoirs, Western Hubei Province, South China", Minerals, vol. 14, no. 1, pp. 10, 2023. https://doi.org/10.3390/min14010010
6. Y. Huang, J. Zhang, P. Zhang, X. Tang, J. Yang, "Multi-scale pore structure characteristics and main controlling factors analysis of Longtan formation shale in Northwest Guizhou", Frontiers in Earth Science, vol. 10, 2023. https://doi.org/10.3389/feart.2022.1033979
7. Z. Li, D. Liu, Y. Cai, Y. Wang, J. Teng, "Adsorption pore structure and its fractal characteristics of coals by N2 adsorption/desorption and FESEM image analyses", Fuel, vol. 257, pp. 116031, 2019. https://doi.org/10.1016/j.fuel.2019.116031
8. Y. Yuan, R. Rezaee, E. A. Al-Khdheeawi, S. Y. Hu, M. Verrall, J. Zou, K. Liu, "Impact of Composition on Pore Structure Properties in Shale: Implications for Micro-/Mesopore Volume and Surface Area Prediction", Energy Fuels, vol. 33, no. 10, pp. 9619-9628, 2019. https://doi.org/10.1021/acs.energyfuels.9b02232
9. X. Shi, W. Wu, L. Xu, L. Xu, Y.Z. Yin, Y.R. Yang, J. Liu, X. Yang, Y. Li, Q. Wu, K. Zhong, Y. Wu, "Thermal Maturity Constraint Effect and Development Model of Shale Pore Structure: A Case Study of Longmaxi Formation Shale in Southern Sichuan Basin, China", Minerals, vol. 14, no. 2, pp. 163, 2024. https://doi.org/10.3390/MIN14020163
10. P. Zhao, B. He, B. Zhang, J. Liu, "Porosity of gas shale: Is the NMR-based measurement reliable?" Petroleum Science, vol. 19, no. 2, pp. 509-517, 2022. https://doi.org/10.1016/j.petsci.2021.12.013
11. X. Hou, J. J. Sheng, "Experimental study on the imbibition mechanism of the Winsor type I surfactant system with ultra-low IFT in oil-wet shale oil reservoirs by NMR", Journal of Petroleum Science and Engineering, vol. 216, pp. 110785, 2022. https://doi.org/10.1016/j.petrol.2022.110785
12. Z. Sun, H. Zhang, Z. Wei, Y. Wang, B. Wu, S. Zhuo, H. Yang, "Effects of slick water fracturing fluid on pore structure and adsorption characteristics of shale reservoir rocks", Journal of Natural Gas Science and Engineering, vol. 51, pp. 27-36, 2018. https://doi.org/10.1016/j.jngse.2017.12.030
13. A. Li, W. Ding, J. He, P. Dai, S. Yin, F. Xie, "Investigation of pore structure and fractal characteristics of organic-rich shale reservoirs: A case study of Lower Cambrian Qiongzhusi formation in Malong block of eastern Yunnan Province, South China", Marine and Petroleum Geology, vol. 70, pp. 46-57, 2016. https://doi.org/10.1016/j.marpetgeo.2015.11.004
14. Z. Li, X. Shen, Z. Qi, R. Hu, "Study on the pore structure and fractal characteristics of marine and continental shale based on mercury porosimetry, N2 adsorption and NMR methods", Journal of Natural Gas Science and Engineering, vol. 53, pp. 12-21, 2018. https://doi.org/10.1016/j.jngse.2018.02.027
15. T. Cao, Z. Song, S. Wang, J. Xia, "Characterization of pore structure and fractal dimension of Paleozoic shales from the northeastern Sichuan Basin, China", Journal of Natural Gas Science and Engineering, vol. 35, no. Part A, pp. 882-895, 2016. https://doi.org/10.1016/j.jngse.2016.09.022

16. S. Wang, Z. Song, T. Cao, X. Song, "The methane sorption capacity of Paleozoic shales from the Sichuan Basin, China", Marine and Petroleum Geology, vol. 44, pp. 112-119, 2013. https://doi.org/10.1016/j.marpetgeo.2013.03.007
17. C. Liang, Z. Jiang, Y.T. Yang, X.J. Wei, "Shale lithofacies and reservoir space of the Wufeng-Longmaxi Formation, Sichuan Basin, China", Petroleum Exploration and Development, vol. 39, no. 6, pp. 736-743, 2012. https://doi.org/10.1016/S1876-3804(12)60098-6
18. D. Avnir, M. Jaroniec, "An Isotherm Equation for Adsorption on Fractal Surfaces of Heterogeneous Porous Materials", Langmuir, vol. 5, no. 6, pp. 1431-1433, 1989. https://doi.org/10.1021/la00090a032
19. H. Huang, R. Li, F. Xiong, H. Hu, W. Sun, Z. Jiang, L. Wu, "A method to probe the pore-throat structure of tight reservoirs based on low- field NMR : Insights from a cylindrical pore model", Marine and Petroleum Geology, vol. 117, pp. 104344, 2020. https://doi.org/10.1016/j.marpetgeo.2020.104344
20. Y. Yao, D. Liu, D. Tang, S. Tang, W. Huang, "Fractal characterization of adsorption-pores of coals from North China : An investigation on CH 4 adsorption capacity of coals", International Journal of Coal Geology, vol. 73, no. 1, pp. 27-42, 2007. https://doi.org/10.1016/j.coal.2007.07.003
21. I. M. Ismail, P. Pfeifer, "Fractal Analysis and Surface Roughness of Nonporous Carbon Fibers and Carbon Blacks", Langmuir, vol. 10, no. 5, pp. 1532-1538, 1994. https://doi.org/10.1021/la00017a035
22. G. Ni, S. Li, S. Rahman, M. Xun, H. Wang, Y. Xu, H. Xie, "Effect of nitric acid on the pore structure and fractal characteristics of coal based on the low-temperature nitrogen adsorption method", Powder Technology, vol. 367, pp. 506-516, 2020. https://doi.org/10.1016/j.powtec.2020.04.011
23. W. Han, G. Zhou, D. Gao, Z. Zhang, Z. Wei, H. Wang, H. Yang, "Experimental analysis of the pore structure and fractal characteristics of different metamorphic coal based on mercury intrusion-nitrogen adsorption porosimetry", Powder Technology, vol. 362, pp. 386-398, 2020. https://doi.org/10.1016/j.powtec.2019.11.092
24. S. Meng, X. Ma, H. Gong, B. Wang, Z. Cui, "Molecular dynamics study of boiling heat transfer in nanochannels under capillary flow", Journal of Molecular Liquids, vol. 395, pp. 123955, 2024. https://doi.org/10.1016/j.molliq.2024.123955
25. Z. Liu, B. Bai, J. Tang, Z. Xiang, S. Zeng, H. Qu, "Investigation of slickwater effect on permeability of gas shale from longmaxi formation", Energy and Fuels, vol. 35, no. 4, pp. 3104-3111, 2021. https://doi.org/10.1021/acs.energyfuels.0c04081
26. Z. Liu, B. Bai, Y. Wang, H. Qu, Q. Xiao, S. Zeng, "Spontaneous imbibition characteristics of slickwater and its components in Longmaxi shale", Journal of Petroleum Science and Engineering, vol. 202, pp. 108599, 2021. https://doi.org/10.1016/j.petrol.2021.108599
27. X. Shao, X. Pang, H. Li, X. Zhang, "Fractal Analysis of Pore Network in Tight Gas Sandstones Using NMR Method: A Case Study from the Ordos Basin, China", Energy and Fuels, vol. 31, no. 10, pp. 10358-10368, 2017. https://doi.org/10.1021/acs.energyfuels.7b01007
28. Z. Liu, B. Bai, Z. Ding, H. Qu, S. Zeng, X. Da, "Impact of cleanup additive on methane desorption on Longmaxi shale", Fuel, vol. 300, pp. 121003, 2020. https://doi.org/10.1016/j.fuel.2021.121003
29. Y. Zhao, Y. Sun, S. Liu, K. Wang, Y. Jiang, "Pore structure characterization of coal by NMR cryoporometry", Fuel, vol. 190, pp. 359-369, 2017. https://doi.org/10.1016/j.fuel.2016.10.121
30. Y. Tian, Q. Chen, C. Yan, H. Deng, Y. He, "Classification of Adsorption Isotherm Curves for Shale Based on Pore Structure", Petrophysics, vol. 61, no. 5, pp. 417-433, 2020. https://doi.org/10.30632/pjv61n5-2020a2
31. X. Guo, Z. Huang, L. Zhao, W. Han, C. Ding, X. Sun, R. Wang, "Pore structure and multi-fractal analysis of tight sandstone using MIP, NMR and NMRC methods: A case study from

the Kuqa depression, China", Journal of Petroleum Science and Engineering, vol. 178, pp. 544-558, 2019. https://doi.org/10.1016/j.petrol.2019.03.069

32. Y. Jiang, Y. Fu, Z. Lei, Y. Gu, L. Qi, Z. Cao, "Experimental NMR Analysis of Oil and Water Imbibition during Fracturing in Longmaxi Shale, SE Sichuan Basin", Journal of the Japan Petroleum Institute, vol. 62, no. 1, pp. 1-10, 2019. https://doi.org/10.1627/jpi.62.1
33. Y. Yuan, R. Rezaee, "Impact of Paramagnetic Minerals on NMR-Converted Pore Size Distributions in Permian Carynginia Shales", Energy and Fuels, vol. 33, no. 4, pp. 2880-2887, 2019. https://doi.org/10.1021/acs.energyfuels.8b04003
34. O. Ozotta, K. Liu, T. Gentzis, H. Carvajal-Ortiz, B. Liu, S. Rafieepour, M. Ostadhassan, "Pore structure alteration of organic-rich shale with SC-CO2 exposure: The Bakken formation", Energy and Fuels, vol. 35, no. 6, pp. 5074-5089, 2021. https://doi.org/10.1021/acs.energyfuels.0c03763
35. W. Sun, Y. Zuo, Z. Wu, H. Liu, S. Xi, Y. Shui, J. Lin, "Fractal analysis of pores and the pore structure of the Lower Cambrian Niutitang shale in northern Guizhou province: Investigations using NMR, SEM and image analyses", Marine and Petroleum Geology, vol. 99, pp. 416-428, 2019. https://doi.org/10.1016/j.marpetgeo.2018.10.042